The formation of fluidized ejecta on Mars by granular flows

Koji WADA[1][*] and Olivier S. BARNOUIN-JHA[2]

[1]Institute of Low Temperature Science, Hokkaido University, N19-W8, Kita-ku, Sapporo 060-0819, Japan
[2]The Johns Hopkins University Applied Physics Laboratory, Johns Hopkins Road, Laurel, Maryland 20723, USA
[*]Corresponding author. E-mail: wada@neko.lowtem.hokudai.ac.jp

Abstract–A simple granular flow model is used to investigate some of the conditions under which ejecta may flow as a granular media. The purpose of this investigation is to provide some bounds as to when either volatiles or an atmosphere are required to explain the fluid-like morphology of many Martian ejecta deposits. We consider the ejecta deposition process from when an ejecta curtain first strikes a target surface via ballistics and possibly flows thereafter. A new finding is that either hard-smooth surfaces or slightly erodible surfaces allow ejecta to flow readily as a granular medium. Neither volatiles nor an atmosphere are required to initiate flow. A low friction coefficient between ejecta grains can also generate flow and would be analogous to adding volatiles to the ejecta. The presence of either a rough or a densely packed erodible surface does not permit easy ejecta flow. High friction coefficients between ejecta grain also prevent flow, while changes in the coefficient of restitution (a measure of how much energy is retained after collisions between particles) plays a minor role in the flow dynamics of ejecta. A hard smooth or a somewhat erodible surface could be generated by past fluvial activity on Mars, which can either indurate a surface, erode and smooth a surface, or generate sedimentary terrains that are fairly easy to erode. No ramparts or layered ejecta morphologies are generated by our model, but this may be because several simplifying assumptions are used in our model and should not be construed as proof that either volatiles or an atmosphere are required to form fluidized ejecta morphologies.

INTRODUCTION

Many ejecta deposits on Mars possess flow-like features (Carr et al. 1977; Mutch and Woronow 1980; Mouginis-Mark 1979; Schultz and Gault 1979). They have long run-out distances that usually exceed the run-out of ejecta seen on other planets (Schultz and Singer 1980; Schultz 1992), and the distal deposits beyond the near-rim region are on average fairly thin (50–100 m) (Barnouin-Jha et al. 2005a; Baloga et al. 2005). They often possess one or more ramparts, which can measure ~200 m in height, at their edges (Barnouin-Jha et al. 2005a; Baloga et al. 2005).

Two main processes have been proposed for the origin of these flows: 1) volatiles (mainly in the form of water or vapor) within the excavated ejecta provide lubrication, which permits easy flow after it reaches the ground (Carr et al. 1977; Mouginis-Mark 1979, 1981; Wohletz and Sheridan 1983; Ivanov 1996); and 2) strong atmospheric winds generated by the impact entrain significant portions of the ejecta that are then deposited as gravity currents (Schultz and Gault 1979, 1982; Schultz 1992; Barnouin-Jha and Schultz 1996, 1998b;

Suzuki et al. 2005). As a third possibility, we propose that Martian fluidized ejecta deposits could be the result of a simple granular flow, i.e., a flow composed of a collection of discrete solid particles.

Modern advances in the understanding of granular flow mechanics indicate that these may well control the formation of long run-out landslides on Earth (Savage and Hutter 1989, 1991; Campbell et al. 1995; Davies and McSaveney 1999) and Mars (Barnouin-Jha et al. 2005a, 2005b), including the formation of distal ramparts. Thus, granular flows may also explain the fluid-like appearance of ejecta deposits seen on the surface of Mars.

However, granular flows have never been seriously considered as an explanation for Martian fluidized ejecta because they are only commonly seen on Mars, and not on the Moon or Mercury. If granular flows are effective in making such deposits, then why are they not also present in abundance on the Moon and Mercury? Such logic has lead authors to prefer either the volatile or atmospheric origin for fluidized ejecta on Mars.

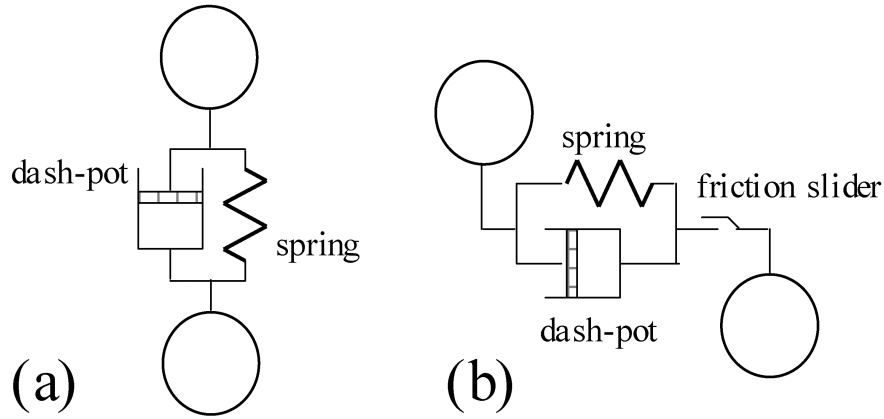A granular flow consideration of the origin of fluidized

Fig. 1. The schematics of the interaction model between contact particles: (a) is normal direction and (b) is tangential direction. The springs simulate the elastic or "bouncing" behavior of the particles, while the dash-pots dissipate collisional energy. The friction-slider allows for tangential friction between the spheres as described by a Coulomb model.

ejecta could indicate that the difference between Mars and Moon and Mercury are simply due to surface conditions. The Martian surface may be either smooth, hard or both allowing ejecta to flow long distances, while the surfaces of the Moon and Mercury could be rough, soft or both not permitting ejecta to flow well. The latter surface conditions on the Moon and Mercury may be expected given their long history of impacts, which should generate a battered and broken up surface, forming a heterogeneous and mixed unconsolidated megaregolith (e.g., Taylor 1982). Although also battered, the Martian surface could have been more effectively sedimented as a consequence of the presence of past volatiles (mainly in the form of water) and a denser atmosphere to form smooth hard surfaces.

In this study, we conduct preliminary 3-D distinct element method (DEM) calculations of the ejecta deposition process to explore the circumstances under which ejecta can flow effectively as a simple granular flow. Because the DEM calculations treat individual particles separately, the results presented are not the result of a continuum formulation as used in other studies (e.g., Barnouin-Jha et al. 2005a; Baloga et al. 2005). While very computer-intensive, a DEM permits the investigation of the motion of individual ejecta within the flow and factors that influence the overall continuum behavior of the flow. The solutions generated by the DEM provide reasonable initial conditions and important references for flow solutions obtained using continuum formulations that are typically easier and less time-intensive to obtain.

In our DEM calculations, we focus especially on a few rheological parameters of the ejecta and surface such as the coefficients of restitution and friction between ejecta particles and surface. We also consider various surface conditions such as whether or not these are smooth, rough, or erodible. The effects of surface softness are evaluated through the use of an erodible surface.

Our models are both simplified and preliminary in that we consider only the dynamics of ejecta comprised of large single-sized spheres. A range of grain sizes, cohesion, and angularity between grains are not included and may play an important role in the emplacement of ejecta and particularly the formation of ramparts. Nevertheless, the results presented do provide a qualitative sense for when ejecta as a simple granular media may be expected to flow and when not. In this way, they help understand or bound those conditions for which other factors such as volatiles and an atmosphere may influence the ejecta deposition process.

NUMERICAL MODEL

Distinct Element Method

Our granular flow model uses the distinct element method (DEM) in three dimensions. This method originated with Cundall and Strack (1979) and is commonly used in a variety of fields (see Cook and Jensen 2002). In geology and planetary science, DEM or DEM-like methods are extensively used to investigate the break-up of comets (Asphaug and Benz 1994), landslide motion (Campbell et al. 1995), dust coagulation (Dominik and Tielens 1997), volcanic spreading (McGovern and Morgan 2005), impact cratering (Wada et al. 2006), accretion of planetesimals (Leinhardt and Richardson 2005), and the breakup of rubble piles (Richardson et al. 2005), to mention a few.

In the model used here, the motions of individual particles are calculated by solving the conservation of linear and angular momentum equations for each particle, taking into account interactions between particles that are in contact. The momentum equations are given by:

$$m_i \ddot{\boldsymbol{x}}_i = \sum_j [\boldsymbol{f}_{n,ij} + \boldsymbol{f}_{s,ij}] + m_i \boldsymbol{g} \qquad (1)$$

$$I_i \dot{\mathbf{w}}_i = \sum_j \boldsymbol{r}_{ij} \times \boldsymbol{f}_{s,ij} \qquad (2)$$
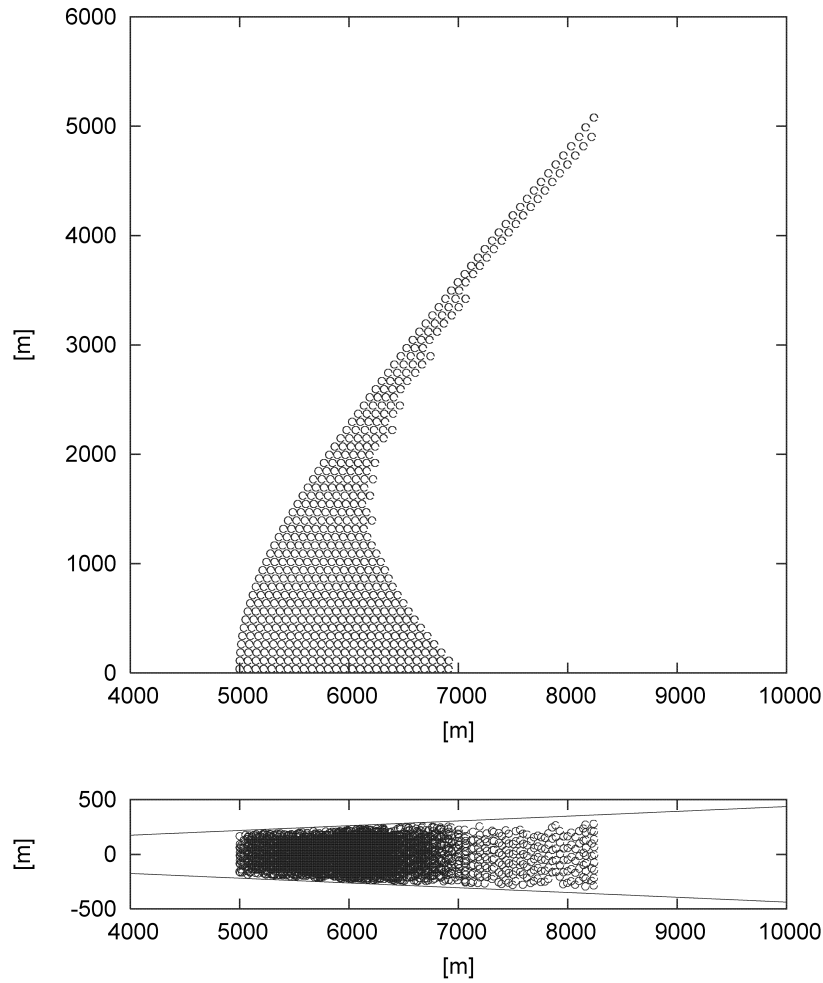
Fig. 2. The initial conditions for the ejecta particles for an ejection angle of 45 degrees: side (top) and top (bottom) views. The horizontal scale indicates the distance from the impact point. Two lines in the top view indicate the boundaries of the calculation region for a 5 degrees ejecta wedge.
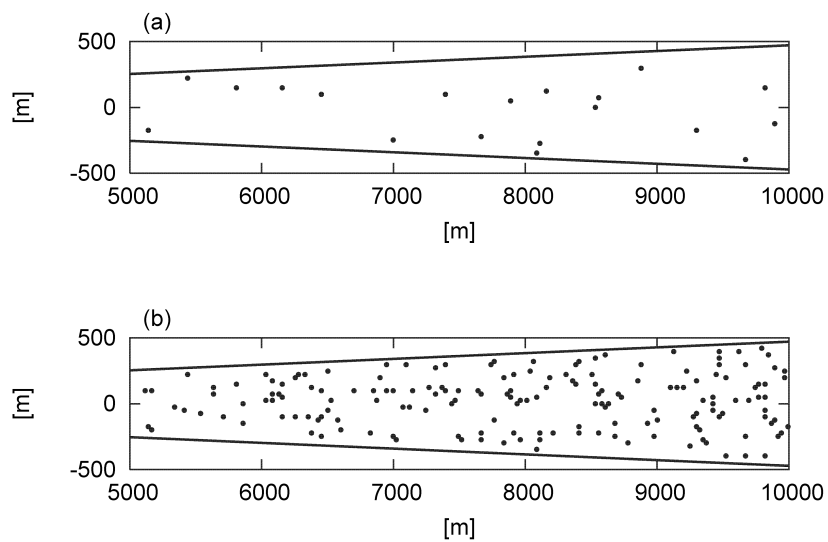

Fig. 3. The top views of (a) low-roughness and (b) high-roughness surfaces. Obstacles are plotted within the calculation region bounded by the lines.
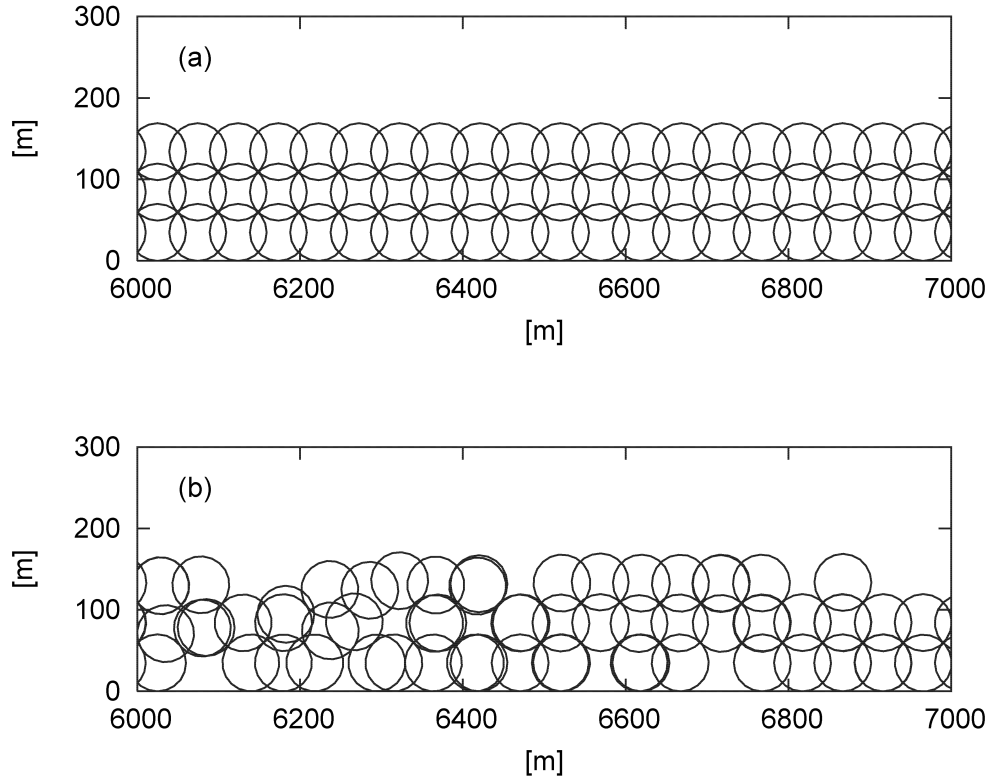
Fig. 4. The cross-sectional side views of (a) erodible and (b) rough-erodible surfaces. Movable particles are represented by circles.

where m_i, I_i, x_i, and $\mathbf{w}_i$ are the mass, the moment of inertia, the position vector, and the angular velocity vector of the particle i, respectively. The variable r_{ij} is defined as $r_{ij} = r_i e_{ij}$, where r_i is the radius of the particle i and e_{ij} is the unit vector that originates from the center of the particle i and is directed toward the center of the particle j, g is the acceleration due to gravity, and $f_{n,ij}$ and $f_{s,ij}$ are the normal and tangential forces on the particle i acted by the particle j. Detailed descriptions on how these latter two forces are estimated are described in Wada et al. (2006). A brief review is given below.

In order to handle the interaction between the particles, we adapt a Voigt model, which consists of a pair of spring and dash-pot for the normal and tangential direction, respectively (Fig. 1). The spring simulates elastic restitution, describing the storage and release of elastic energy that occurs during a collision. The dash-pot acts like a shock absorber, dissipating energy during contact. A friction-slider model is also introduced in the tangential direction, taking into account friction losses between sliding particles via Coulomb friction. In our model, particles are assumed to be single-size spheres with radius r. These are nondeformable but can overlap a bit with each other. The magnitude of the interaction forces can be calculated using the overlapping length. If the friction-slider model is not included, the normal and tangential interaction forces $f_{n,ij}$ and $f_{s,ij}$ are given by:

$$f_{n,\,ij} = -\sum k_n \Delta d_{n,\,ij} - \eta_n v_{n,\,ij} \qquad (3)$$

$$f_{s,\,ij} = -\sum k_s \Delta d_{s,\,ij} - \eta_s v_{s,\,ij} \qquad (4)$$

where $k_{n/s}$ is the stiffness of the spring, $\eta_{n/s}$ is the dash-pot coefficient, $\Delta d_{n/s,ij}$ is the change of relative displacement of contact particle pair i and j during each time step, and $v_{n/s,ij}$ is the relative velocity of the contact particle pair. As we will see below, the value of $k_{n/s}$ changes with time. The elastic force generated during contact is given by the summation of $k_{n/s}\Delta d_{n/s,ij}$ at each time step from when contact first occurs.

In this study, we adapt Hertzian contact theory (e.g., Johnson 1987) to give the stiffness k_n:

$$k_n = \frac{2E}{3(1-v^2)}\left(\frac{3}{4}\frac{1-v^2}{E}rP\right)^{\frac{1}{3}} \qquad (5)$$

where E is the Young's modulus, v is the Poisson's ratio, r is the particle radius, and P is the elastic force (i.e., the first term on the right-hand side of Equation 3) obtained at the previous time step. For the interaction with walls, the normal stiffness k_{nw} is also given by:

$$k_{nw} = \frac{2E}{3(1-v^2)}\left(\frac{3}{2}\frac{1-v^2}{E}rP\right)^{\frac{1}{3}} \qquad (6)$$

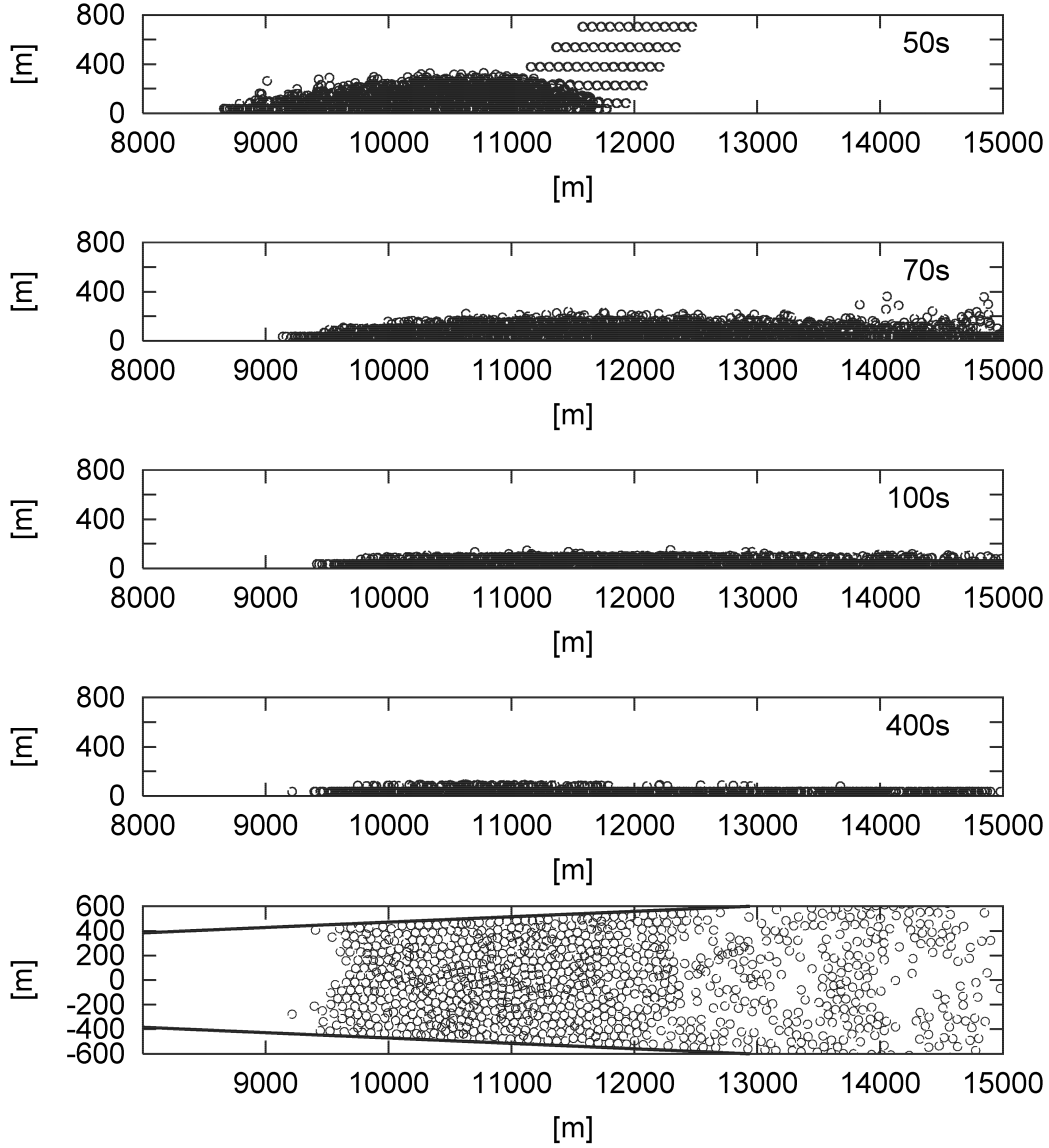Assuming that the ratio of stiffness k_s/k_n is equivalent to

Fig. 5. The first four figures show side-view snapshots of ejecta flow on a smooth surface ($e = 0.1$, $\mu = 0.5$) with a 45-degree ejection angle. Each snapshot is labeled with the time from when the calculation was begun. The bottom figure shows a top view of the ejecta deposit at 400 s when most particle motion stops. The horizontal scale indicates the distance from the impact point.

the ratio between shear and longitudinal elastic moduli, $G/E = 1/(2(1 + v))$, the tangential stiffness k_s (and k_{sw} for the interaction with walls) is given by:

$$k_s = \frac{1}{2(1+v)}k_n \qquad (7)$$

$$k_{sw} = \frac{1}{2(1+v)}k_{nw} \qquad (8)$$

The dash-pot coefficient $\eta_{n/s}$ is determined using a coefficient of restitution e, which we derive from a linear one-dimensional model (Duran 2000) of oscillation damping:

$$m\ddot{\xi} = -k_n\xi - \eta_n\dot{\xi} \qquad (9)$$

where $m = m_i/2$ is the reduced mass of two contact particles and ξ is the relative displacement of the two particles. The value of e is then analytically derived as:

$$e = \exp\left(-\pi\frac{\eta_n}{\sqrt{4mk_n - \eta_n^2}}\right) \qquad (10)$$

and gives η_n:

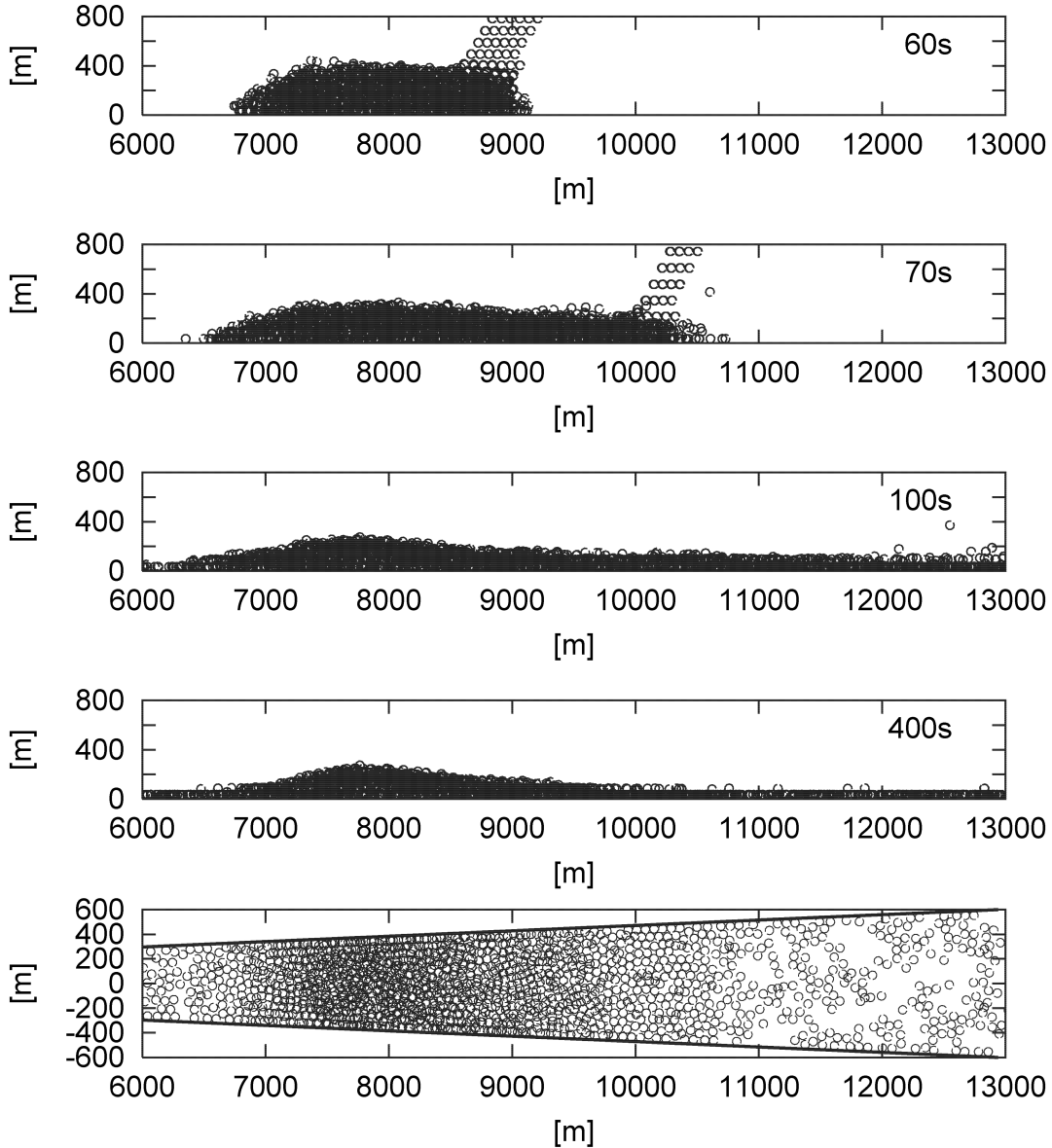$$\eta_n = 2\sqrt{\frac{mk_n}{1 + (\pi/\ln e)^2}} \qquad (11)$$

Fig. 6. The same as Fig. 5, except with a 70-degree ejection angle.

For the tangential direction, η_s possess the same form:

$$\eta_s = 2\sqrt{\frac{mk_s}{1 + (\pi/\ln e)^2}} \qquad (12)$$

In the case of collision between a particle and a wall, we also use these dash-pot coefficients, but replace m with the mass of particle m_i.

Although in general the coefficient of restitution e is dependent on the collision velocity, e becomes independent of this collisional velocity by using the linear damping model. We therefore treat e as a parameter for energy dissipation.

The frictional force between particles (and between the particles and walls) is basically given by the tangential force

$f_{s,ij}$ calculated using the above procedure. When the tangential elastic force becomes greater than the normal elastic force multiplied by the coefficient of friction μ, i.e.:

$$\left|\sum k_s \Delta d_{s,ij}\right| > \mu \sum k_n \Delta d_{n,ij} \qquad (13)$$

the friction slider works to cut off the tangential force and the absolute value of tangential friction is given by $\mu \sum k_n \Delta d_{n,ij}$. Both static and kinetic frictions can be described by this friction model. However, for the sake of simplicity, we use only one value of μ to describe both of these friction states.

Thus, in our model two parameters—the coefficient of restitution e and the coefficient of friction μ—parameterize energy losses due to collision and friction, respectively.
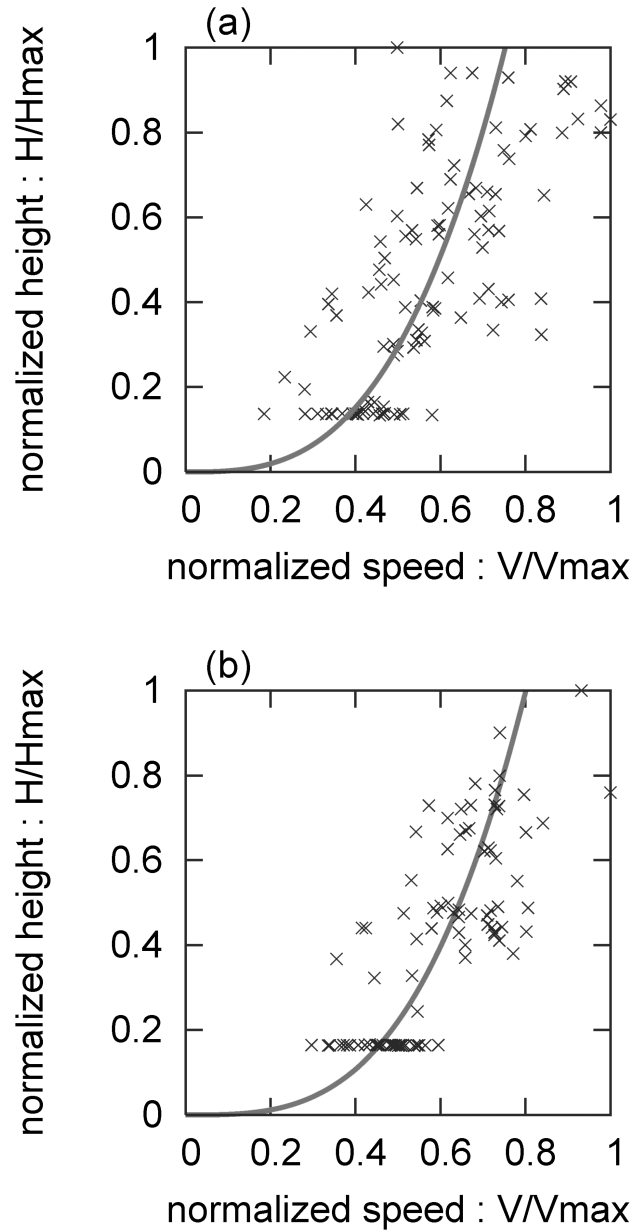
Fig. 7. The velocity profiles for ejecta flow on a smooth surface with an ejection angle of (a) 70 degrees and (b) 45 degrees. Both profiles are taken 70 s after the start of the calculation, but at a horizontal distance of (a) 9000 ± 100 m and (b) 11000 ± 100 m. Plotted curves are fit to the data.

Our DEM has been previously applied to investigate the impact cratering process on dry granular materials (Wada et al. 2006) and the results are consistent with laboratory impact experiments. We have also applied our code to the analysis of landslide motions (Barnouin-Jha et al. 2005b) and obtained helpful insights. However, since rolling resistance due to angularity of particles is not present in our model and the particles do not fracture or deform, it is not easy to pile up our single-size spheres to create significant topography, as they prefer to roll unimpeded (Duran 2000). The lack of range of grain sizes and use of a small number of particles may

contribute to this problem. In the future, we plan to introduce a greater number of particles with various sizes and appropriate rolling resistance and fracturing in order to investigate how these factors may contribute to the generation of fluidized ejecta morphologies.

Initial Conditions and Particle Parameters

As an initial condition of our DEM calculations, we consider a wedge of an ejecta curtain composed of particles each traveling on ballistic paths prior to deposition (Fig. 2).
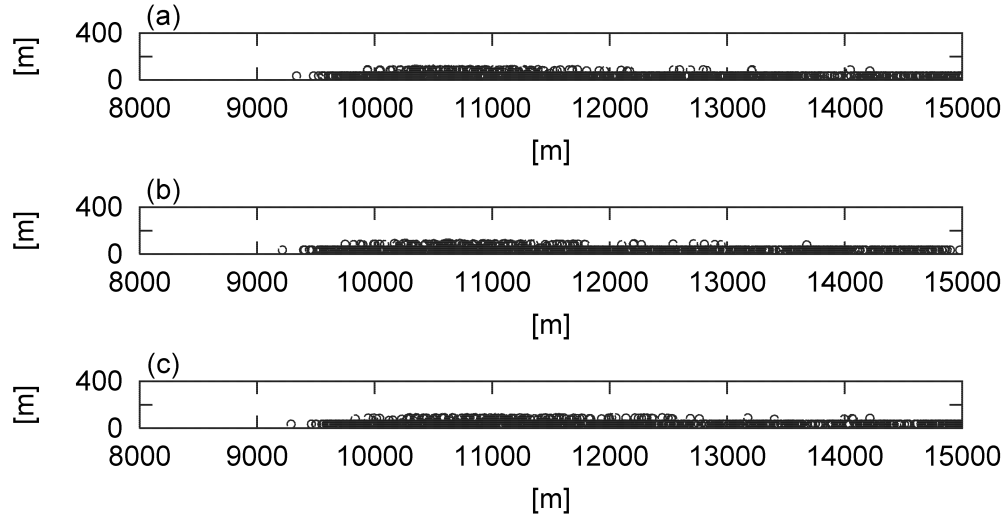
Fig. 8. The side views of ejecta deposit on a smooth surface for three different values of the coefficient of restitution e: (a) $e = 0.4$; (b) $e = 0.1$; and (c) $e = 0.01$. The coefficient of friction is kept constant at $\mu = 0.5$.

To save on computer memory and calculation time, all our computations use a 5-degree-wide wedge after it was determined that using larger sections of the ejecta curtain had little influence on the computed results.

Each ejecta wedge was obtained using the crater scaling rules (Housen et al. 1983). These models use empirically derived constants to provide an estimate of the volume of ejecta excavated as a function of position and ejection velocity for a transient crater. We use the version of the crater scaling rule that assumes that target strength is a minor contributor in the dynamics of crater formation relative to gravity. The computed ejecta volume can be converted into a number of ejecta particles at a given position in an ejecta curtain given a particle diameter. We place these particles randomly in the curtain, ensuring that they do not come in contact with each other (see Appendix for more detail).

Figure 2 shows the initial particle distribution for one of our simulated ejecta curtain wedges. In all the results presented, we consider a transient crater 10 km in diameter on Mars with spherical ejecta particles 70 m in diameter. This resulted in an ejecta curtain wedge comprised of 3,000 particles.

As part of this study, we considered ejecta curtains formed using two different ejection angles: one with 45 degrees (normal ejection angle) and the other with 70 degrees (high ejection angle). The ejection angle is defined as that angle at which ejecta particles are launched from the original target plane. The first angle would simulate impact under normal surface conditions, while the second could be the result of impacts in a volatile-rich surface. Indeed, both numerical (Stewart et al. 2001) and laboratory (Greeley et al. 1980) results indicate that ejection angles tend to be higher in case of an impact into water-rich target.

Each ejecta particle comprising our curtain has material properties of quartz, i.e., a density of 2.7 gcm^{-3}, a Young's modulus of 9.4×10^{10} Pa, and Poisson's ratio of 0.17. As part of our numerical investigation, we investigated the effect of changing the coefficients of restitution e and friction μ between contact particles. The values of e studied equal 0.01, 0.1, and 0.4; the values of μ equal 0.1, 0.5, and 0.8. Very small values of μ are conceptually equivalent to adding volatiles to the ejecta.

Surface Conditions

The simplest surface considered in our investigations is the smooth, flat plain. In addition, we also consider three other types of surfaces: a rough, an erodible, and a rough-erodible surface.

To form the rough surface, we randomly place on a smooth surface small particles whose sizes are half that of the ejecta (see Fig. 3). These particles are fixed during the calculations and thus become obstacles to ejecta flow. We prepared surfaces with both a high and low roughness, the difference between them being the number density of obstacles. In the roughest version, the number density of obstacles is about 10 times larger than in the low roughness case (Fig. 3). We define the roughness λ using:

$$\lambda = n\pi r_o^2 \frac{r_o}{r} \tag{14}$$

where n is the surface number density of the obstacle particles, r_o is the radius of the obstacle particles, and r is the radius of the ejecta particles. In the case of high surface roughness, $n = 48$ km^{-2}, $r_o = 0.5r = 17.5$ m, and $\lambda = 0.023$. For the low roughness surface $n = 4.7$ km^{-2}, leading to $\lambda = 0.0023$.
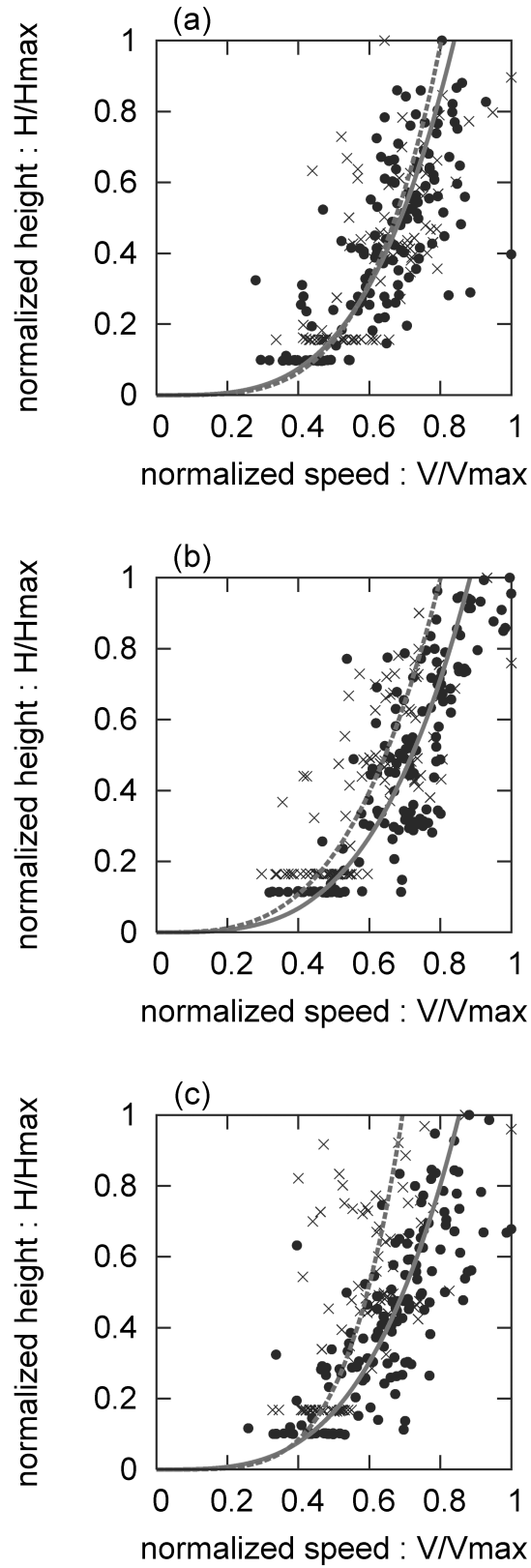
Fig. 9. The velocity profiles for ejecta flow on a smooth surface at the horizontal distance of 11,000 ± 100 m, at the 50 s (black circles with solid fitted curves) and 70 s (x's with dashed fitted curves) after the start of the calculation. The three figures are for the cases of (a) $e = 0.4$; (b) $e = 0.1$; and (c) $e = 0.01$, respectively. $\mu = 0.5$ for all cases.
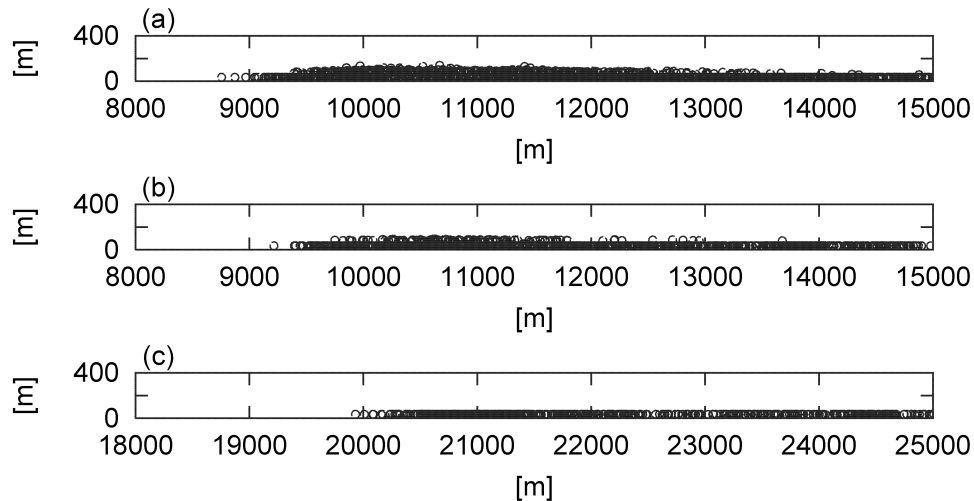
Fig. 10. The side views of ejecta deposit on a smooth surface. The coefficient of friction μ is different in each case: (a) μ = 0.8; (b) μ = 0.5; and (c) μ = 0.1. The coefficient of restitution is kept constant at *e* = 0.1.

In order to create an erodible surface, we place particles of the same size as the ejecta, in dense packing on the surface plain (Fig. 4a). These particles are free to move when ejecta hits them. The total thickness of the particle layer is 169 m.

The rough-erodible surface considered is similar to the erodible one, but the total number of particle is reduced by about 30%, creating a rather loosely packed and uneven or rough surface (Fig. 4b).

NUMERICAL RESULTS

Flow on a Smooth Surface

Figure 5 shows a typical example of how ejecta flows on a smooth surface. This particular example is for a transient crater 10 km in diameter, which after modification may be as large as 15 km. The results show that ejecta flows readily as a granular media. Indeed, the initially thick deposit slowly thins as time proceeds and ejecta are spread out over a larger surface area. Some lobateness or sinuosity is visible at the edge of the continuous portion of the curtain which ends near 12,500 m (Fig. 5, top) and could resemble that seen on Mars (Barlow 1994; Barnouin-Jha and Schultz 1998a). The top view also indicates how several layers of ejecta could be formed during ejecta deposition, with a thicker interior flow and a thinner more dispersed distal flow. In addition, many of the side views at ~70 s show evidence for a distal surge that can be created by distal ejecta which could be the precursor to the continuum flows that generates a pronounced distal rampart.

The ejecta in our models probably flow too efficiently. In fact, our model tends to form unrealistically thin ejecta. The final near-rim thickness is only ~2 particles thick (i.e., ~140 m), which is far thinner than comparable deposits on Mars (Barnouin-Jha et al. 2005a). Although these

calculations may indicate how complex layered ejecta seen on Mars could be formed, none are obviously formed in this study. This is in large part due to the idealizations used in the calculations. Our spherical particles have no rolling resistance or angularity and keep rolling on a smooth surface. In addition, large number of particles, their size distribution, and the fact that they fracture are known to influence the mechanics of granular flows (Midi 2004; Dartevelle 2004; Davies and McSaveney 1999), all of which are not modeled here. All these contributing factors could explain why neither near rim moats nor ramparts are formed in our calculations, both of which are commonly seen at many Martian craters (Mouginis-Mark 1979; Schultz 1992; Barnouin-Jha et al. 2005a). A key contributor could be the surrounding atmosphere, which may actually allow particles in the flow to remain closer together through drag than what is seen in the calculation presented here, and generate more continuum flow-like conditions that naturally generate some of the observed structures on Mars. In the future, we plan to investigate what conditions could lead to the formation of such structures using more realistic models of ejecta. But those would be studies of how granular ejecta flows stop. In this investigation, we focus only on those factors which contribute to the initiation of ejecta flow as a simple granular media.

In the following sections, we show the influence of excavation angle, *e*, μ, surface roughness, and surface softness on the flow dynamics and final morphology of ejecta.

Because of the discrete nature of granular media, the definition of the velocity profile can be confusing. We define this as the velocity of each particle passing through a region at a given instance in time as a function of the vertical height. These values are scaled by their maximum velocity and height. If the profile increases slowly with height (less steep), this indicates a shear flow (Campbell 1990; Campbell et al.
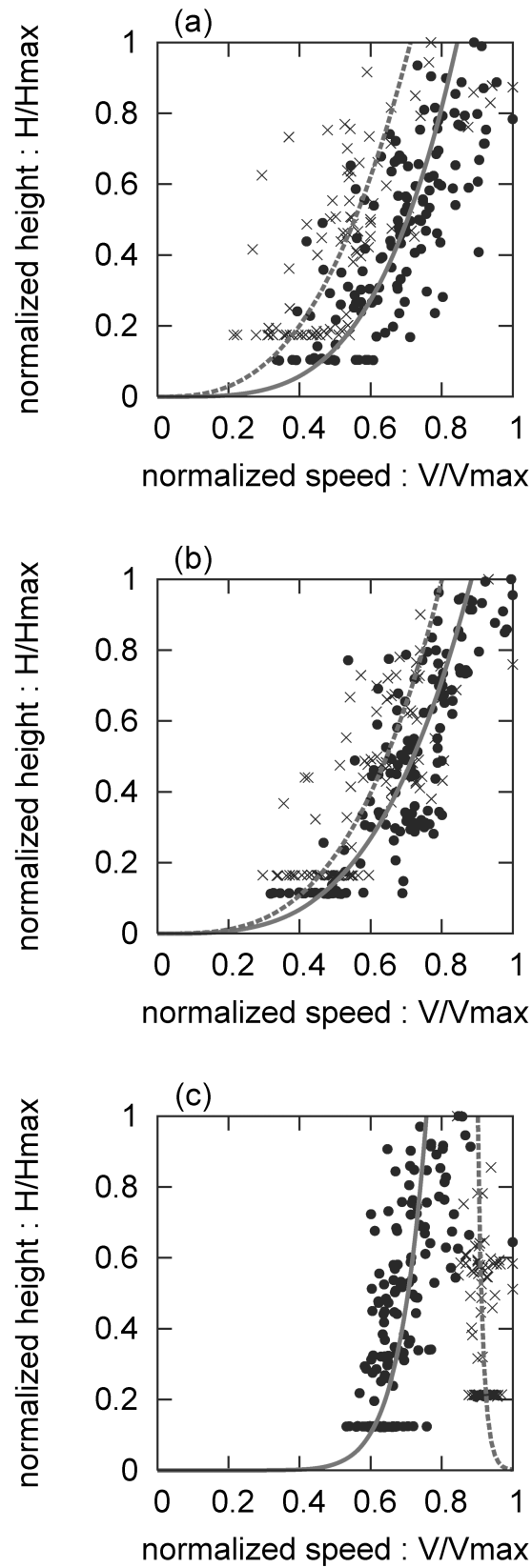
Fig. 11. The velocity profiles of ejecta flow on a smooth surface at the same location and times as in Fig. 9, except that (a) $\mu = 0.8$; (b) $\mu = 0.5$; and (c) $\mu = 0.1$, respectively. $e = 0.1$ for all cases.
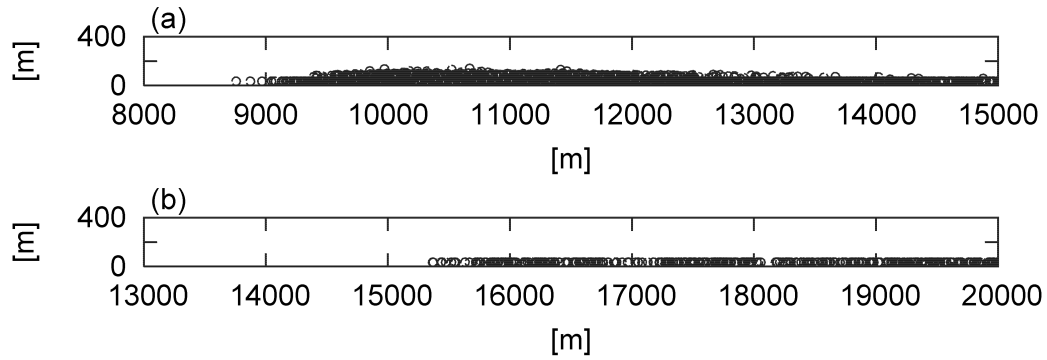
Fig. 12. The side views of ejecta deposit on a smooth surface. The coefficient of friction between ejecta particles is $\mu = 0.8$, while the coefficient of friction between ejecta particles and the surface is different: (a) $\mu_b = 0.8$ and (b) $\mu_b = 0.1$. The coefficient of restitution is $e = 0.1$ for both cases.
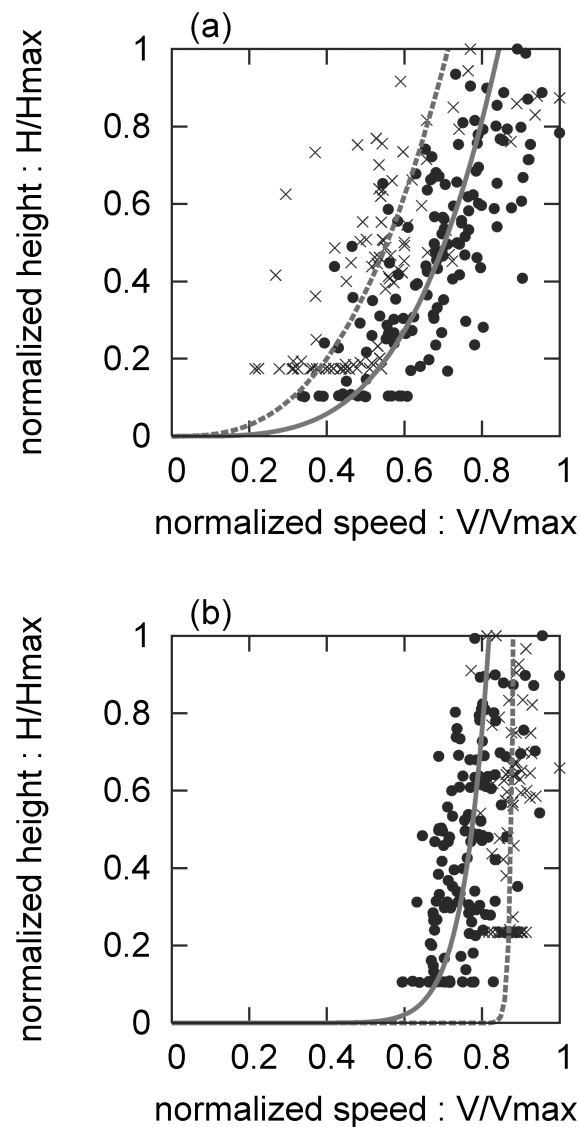

Fig. 13. The velocity profiles of ejecta flow on the smooth surface at the same location and times as in Fig. 9, except that here (a) $\mu = \mu_b = 0.8$; and (b) $\mu = 0.8$, $\mu_b = 0.1$, respectively. $e = 0.1$ for all cases.
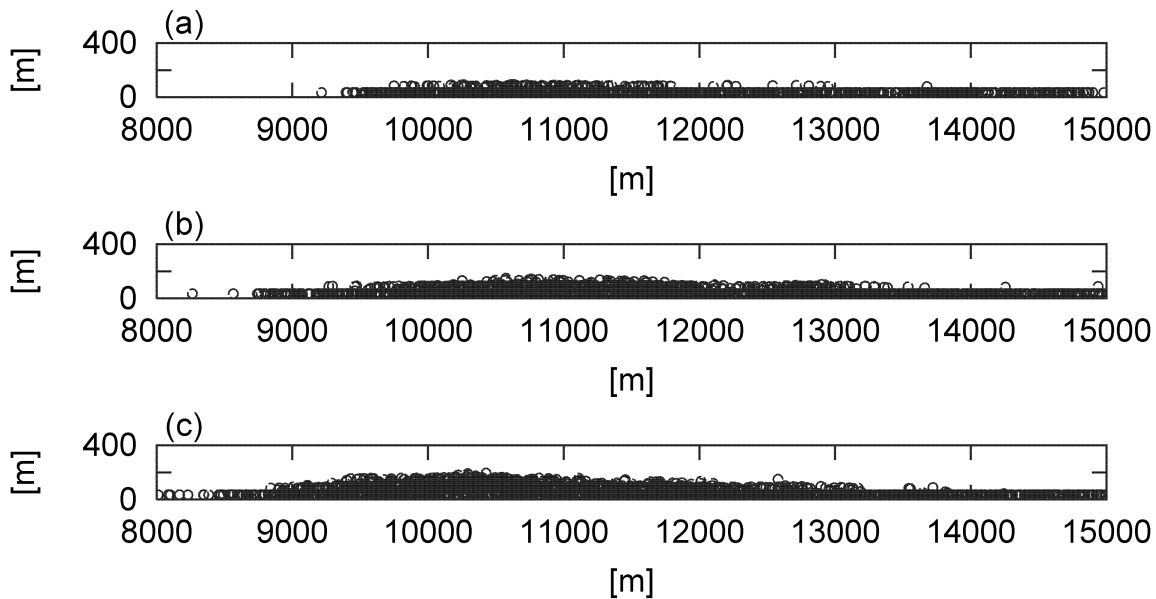
Fig. 14. The side views of ejecta deposit on a (a) smooth, (b) low-roughness, and (c) high-roughness surface. Coefficients of restitution and friction are $e = 0.1$ and $\mu = 0.5$, respectively.

1995). This means that energy is dissipated throughout the flow by shear. In contrast, a near-vertical (steep) velocity profile suggests that shear is not effective in ejecta flow and energy dissipation occurs only at the base of the flow. This latter case would be equivalent to basal glide flows described by Barnouin-Jha et al. (2005a), which are expected to proceed further because energy losses are limited to a small region within the flow.

Excavation Angle

Changing the excavation angle strongly influenced the run-out distances. In the case of the high 70-degree excavation angle, far more ejecta was deposited near-rim, and the ejecta flow forward was far less than for the 45-degree case (Fig. 6). The velocity profiles are also slightly less steep in the 70-degree case relative to the nominal 45-degree case (Fig. 7). Therefore, higher excavation angles ensure that more ejecta is deposited near-rim and that less of it can flow outward. This is because the outward-horizontal component of the kinetic energy that the ejecta possesses reduces with increasing excavation angle. Hence, wet targets could potentially reduce ejecta run-out efficiency if we ignore the influence of water on the internal properties (parameterized here by the terms e and μ) of the ejecta.

Coefficient of Restitution e

Figures 8 and 9 show the shape of the ejecta deposit and velocity profiles for three values of $e = 0.4$, 0.1 and 0.01. The friction coefficient μ is kept constant at 0.5. Smaller values of e imply that the particles lose more energy or stick together

during collision. Values of 0.2–1.0 are not uncommon for steel and ice spheres (Johnson 1987; Bridges et al. 1984). Values near 0.1 may be suitable for rocks (Campbell et al. 1995), as rock collisions tend to be inelastic, perhaps because of internal fractures effectively dissipating collisional energy.

Subtle differences are observed between the shape of the ejecta deposits and the velocity profiles as a function of e. Slightly thicker flows are observed with increasing e, and some evolution from a shear dominated flow to a basal dominated flow are observed. However, in comparison to the effects of μ, surface roughness and erodibility (more below) these effects are small. This lack of difference indicates that, at least on smooth surfaces—and probably all surfaces—changes in the coefficient of restitution have a minor effect on ejecta flow dynamics, implying that energy dissipation due to collisions between individual particles are not very important.

Coefficient of Friction μ

Figure 10 shows three ejecta deposits generated for $\mu =$ 0.8, 0.5, and 0.1. For crustal rocks, typical values of static μ are in the range 0.6–0.75 (Byerlee 1978). The low 0.1 value of μ could represent a wet ejecta flow, although this is not a requirement. Many dry landslides (Hayashi and Self 1992) and earthquakes (Henyey and Wasserburg 1971) indicate that μ can be less than 0.2 without necessarily invoking the presence of water directly.

Unlike e, our results indicate that the coefficient of friction μ between ejecta particles (and surface) strongly influence ejecta flow. As time proceeds, ejecta with the high value of μ do not flow well. On the other hand, the two lower
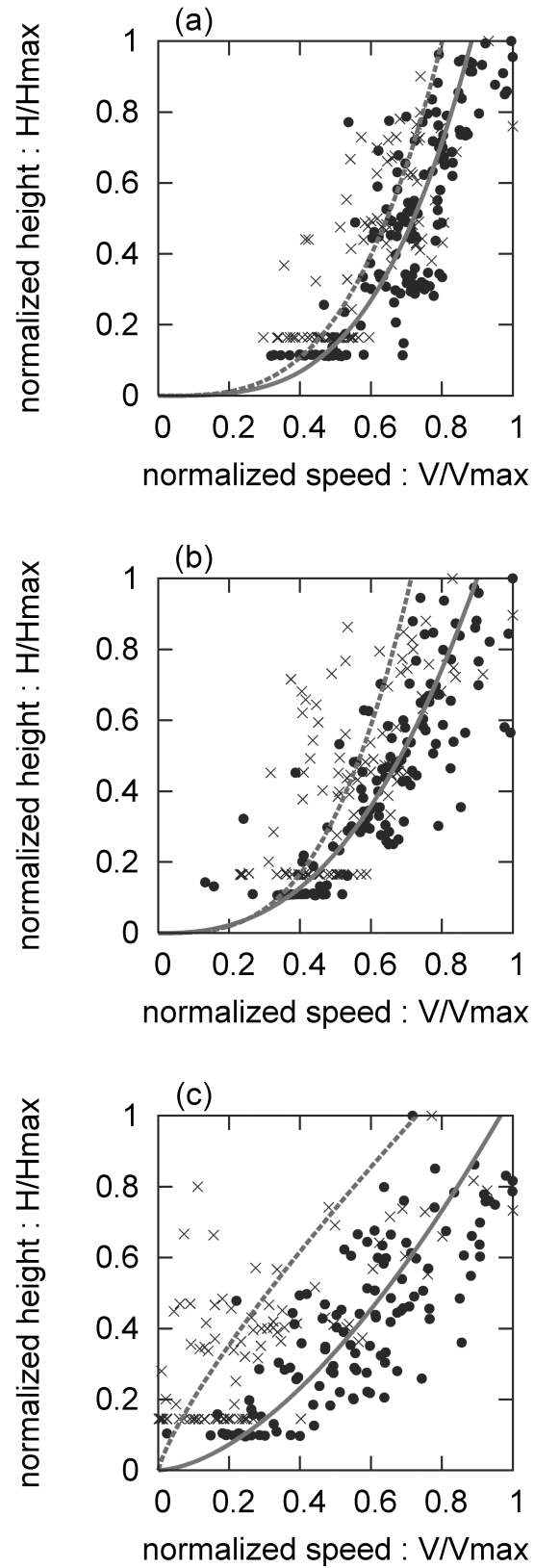
Fig. 15. The velocity profiles of ejecta flow at the same location and times as in Fig. 9, on the (a) smooth, (b) low-roughness, and (c) high-roughness surfaces. $e = 0.1$ and $\mu = 0.5$ for all the cases.
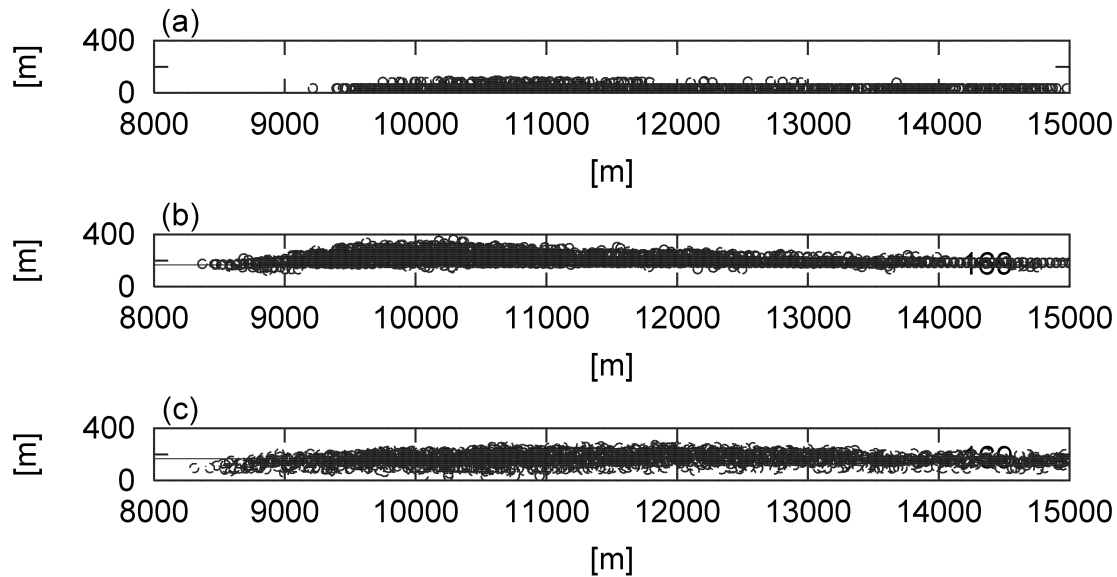
Fig. 16. The side views of ejecta deposit on the (a) smooth, (b) erodible, and (c) rough-erodible surfaces. The coefficients of restitution and friction are $e = 0.1$ and $\mu = 0.5$, respectively. The horizontal line drawn in (b) and (c) indicates the height of original surface, which is composed of movable particles.

μ values show effective ejecta flow, with enhancement of ejecta run-out. Reduction of flow viscosity by adding volatiles could thus explain ejecta flows on Mars, although the presence of a smooth surface or a soft erodible surface are equally viable candidates as we will see below.

The velocity profiles (Fig. 11) also indicate clear differences. The profiles show a reduction in steepness as μ increases, starting at a near-vertical flat when μ is small. These results indicate that much more energy is dissipated throughout the flow via shear at high μ, thereby causing the ejecta particles to pile up and stop more effectively. For the frictionless cases, energy dissipation within the flow is small. Most losses occur at the base and the ejecta particles spread further.

When the coefficient of friction of the surface μ_b is changed, the morphological appearance of ejecta deposits are further influenced (Fig. 12). When the surface friction is low but the friction between ejecta particles remains high (i.e., low μ_b and high μ), ejecta flows well and the velocity profiles become flat (Fig. 13). Not surprisingly, this implies that smooth surfaces allow ejecta to flow further with less energy dissipation.

Surface Roughness

In order to investigate the effects of surface roughness, we show three ejecta deposits in Fig. 14 generated as a result of flow on a smooth surface, a low-roughness surface, and a high-roughness surface. The coefficient of restitution and friction are kept constant at $e = 0.1$ and $\mu = 0.5$. While the ejecta morphologies are nearly identical when first deposited, their appearance differs with surface properties as time proceeds. The rougher the surface is, the more the ejecta pile up and concentrate near the crater rim.

Such a clear trend is also seen in the velocity profiles (Fig. 15). The rough surface generates shallower slopes relative to the smooth surface case, which is nearly vertical. Hence, ejecta deposited on rough surface dissipate energy more efficiently relative to a smooth surface, and the ejecta do not flow as well.

Surface Softness

The influence of surface softness can be analyzed by comparing ejecta flows on a smooth surface, on an erodible surface, and on a rough-erodible surface. Figure 16 shows the ejecta deposits for each one of these cases for $e = 0.1$ and $\mu = 0.5$. On the erodible surfaces, ejecta flows stop sooner. Ejecta run-out is reduced and thicker deposits are observed near-rim.

Consistent with these results, the velocity profiles (Fig. 17) possess smaller slopes than in the erodible cases relative to the smooth surface case. Soft and erodible surfaces are thus more effective in stopping ejecta flow rapidly because of enhanced energy dissipation primarily by shear, leading to shorter run-outs.

Comparison between the erodible and rough-erodible results is of interest. The run-out on the erodible surface is clearly less than in the rough-erodible case (Fig. 16) and the velocity profiles are less steep. These results indicate that our nomenclature "rough-erodible surface" may in fact be a misnomer, and would be better described by a loosely packed soft surface.

Additional analyses show that in the case of the erodible surface, particles are difficult to move due to the dense
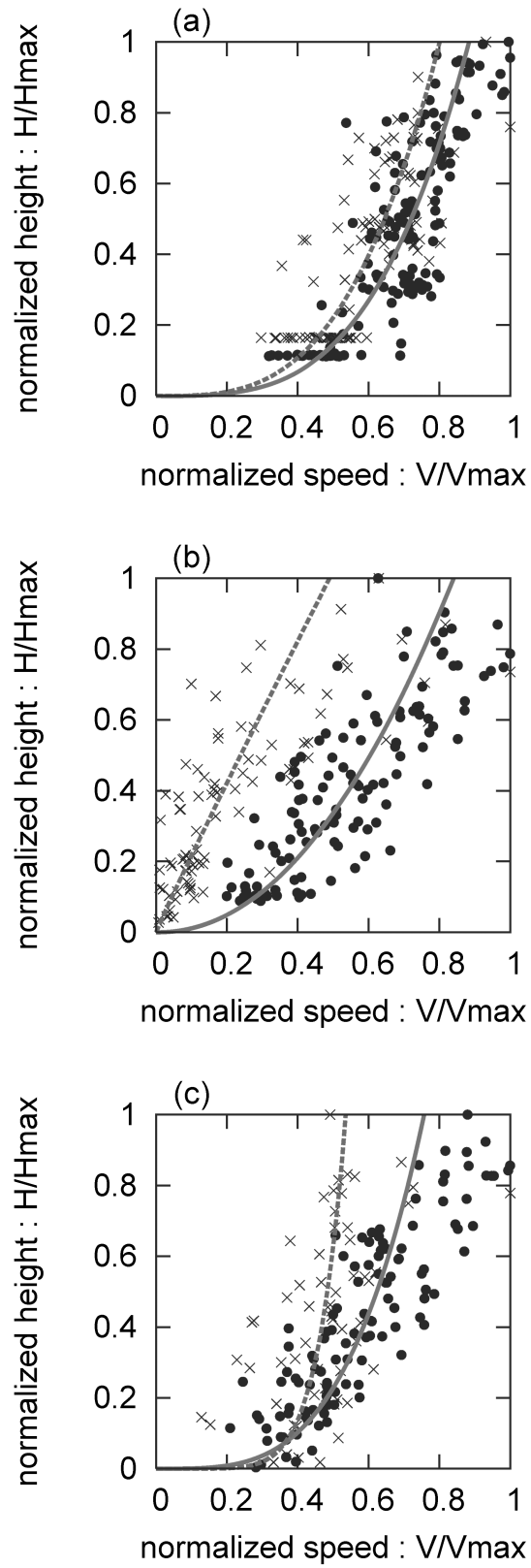
Fig. 17. The velocity profiles of ejecta flow, at the same location and times as in Fig. 9, on the (a) smooth, (b) erodible, and (c) rough-erodible surfaces. $e = 0.1$ and $\mu = 0.5$ for all the cases. In the case of erodible and rough-erodible surfaces, only the ejecta particles above the original surface (i.e., height > 169 m) are plotted.

packing of the surface particles. Falling ejecta is unable to push the pre-existing target material forward, losing much of its initial energy during secondary impact. This leads to the low slopes in the velocity profiles seen for the erodible surface case and short run-outs.

On the other hand, the particles of the soft surface are easier to move. The kinetic energy of the falling ejecta is sufficient to displace and erode the surface particles, permitting ejecta to flow more readily. The steeper velocity profile is generated, whereby less energy is lost in the flow relative to the erodible surface, enhancing run-out.

It is expected that a very loosely packed surface with a lot of porosity may absorb the energy of the ejecta very efficiently, and cause any ejecta flow to stop. In future studies, we will explore this possibility.

SUMMARY OF RESULTS

Our granular flow calculations show that:

• Ejecta can flow readily as a granular media on surfaces that are smooth-hard and nonerodible, or moderately loosely packed (soft) and erodible. Neither water nor atmosphere is required.

• Ejecta flow as a granular media is nearly but not entirely independent of the coefficient of restitution *e*. This implies that energy losses through collisions between ejecta particles are not very important.

• The coefficient of friction μ between both the particles and the surface, surface roughness and surface packing can strongly influence ejecta flows. High μ values, rough, and well-packed (hard) but erodible surfaces can efficiently dissipate the energy of ejecta and rapidly stop flow.

• Increasing the excavation angle, which may occur if the target is wet, tends to reduce run-out, as most ejecta is deposited near the rim, nearly vertically.

• Ramparts and moats are not readily reproduced in our model. This may be due to a number of simplifications assumed in the model, which include lack of rolling resistance due to the angularity of ejecta particles, too small a number of ejecta particle in the flow, lack of differing grains sizes, and lack of fragmentation.

DISCUSSION AND IMPLICATION

Our simple granular flow model results indicate that ejecta flows can be formed on a smooth-hard surface, or on a soft moderately densely packed and erodible surface. The existence of fluidized ejecta deposits on Mars could thus indicate the presence of a very smooth but hard surface, or slightly softer and erodible surfaces. The broad range of run-outs, distal ejecta sinuosity, and even morphological appearance could be due to differences in surface erodibility, or smoothness.

Both smooth but hard surfaces as well as moderately loosely packed and erodible surfaces on Mars could be indicative of the past presence of water. This water could have, for example, indurated some surfaces through sedimentation processes. Tough terrestrial caliches could be a good analog for such possible surfaces. Water could also have removed surface ruggedness by erosion to create smooth regions, and generate sedimentary regions with surfaces that are soft enough (but not too soft and absorbing) to be easily eroded and moved as part of a granular ejecta flow.

On the Moon, the lunar regolith/megaregolith may be too rough or too densely packed to be easily eroded. Ejecta would not flow well in either of these cases. Extensive seismic shaking, which could lead to efficient packing of the lunar regolith/megaregolith, and rugged terrains created by impacts could create these types of surface conditions.

While our calculation show that pre-existing surface properties may be very important and can dominate ejecta flow process, low values in the coefficient of friction may also cause ejecta to flow. Our model results, therefore, indicate that when fluidized ejecta is seen, volatiles could be responsible for lubricating (reducing μ) ejecta, although their presence is not required.

The fact that our granular model cannot yet generate ramparts, moats, and the generally complex geomorphology seen at many fluidized craters could indicate that either an atmosphere or water must affect ejecta emplacement during crater formation. However, many of these morphological attributes are typically created in mass movements that have a large number of particles (Midi 2004) or when they cease to flow (Iverson 1997; Baloga et al. 2005). Our current simple model lacks both a large number of particles and many of the important components (e.g., lack of grain angularity or no fragmentation) which are required to describe the mechanics that stop flow. Such a conclusion would therefore be premature. In addition, the presence of an atmosphere could also be vital to bring individual ejecta grains together to produce a continuum flow that often generate naturally (Baloga et al. 2005; Baloga and Barnouin-Jha 2006) many of the flow structures seen at Mars craters.

REFERENCES

Asphaug E. and Benz W. 1994. Density of comet Shoemaker-Levy-9 deduced by modeling breakup of the parent rubble pile. *Nature* 370:120–124.

Baloga S. M. and Barnouin-Jha O. S. 2006. Formation of Mars impact crater ramparts by volatile degassing of the overland ejecta flow (abstract #1309). 37th Lunar and Planetary Science Conference. CD-ROM.

Baloga S. M., Fagents S. A., and Mouginis-Mark P. J. 2005. Emplacement of Martian rampart crater deposits. *Journal of Geophysical Research* 110, doi:2005JGRE.11010001B.

Barlow N. G. 1994. Sinuosity of Martian rampart ejecta deposits. *Journal of Geophysical Research* 99:10,927–10,935.

Barnouin-Jha O. S. and Schultz P. H. 1996. Ejecta entrainment by impact-generated ring vortices: Theory and experiments. *Journal of Geophysical Research* 101:21,099–21,116.

Barnouin-Jha O. S. and Schultz P. H. 1998a. Lobateness of impact ejecta deposits from atmospheric interactions. *Journal of Geophysical Research* 103:25,739–25,756.

Barnouin-Jha O. S. and Schultz P. H. 1998b. Modeling an ejecta curtain in an atmosphere at laboratory scales (abstract #1517). 29th Lunar and Planetary Science Conference. CD-ROM.

Barnouin-Jha O. S., Baloga S., and Glaze L. 2005a. Comparing landslides to fluidized crater ejecta on Mars. *Journal of Geophysical Research* 110, doi:2005JGRE.11004010B.

Barnouin-Jha O. S., Wada K., Matsui T., and Sugita S. 2005b. The flow dynamics of long run-out landslides on Mars from 3-D granular flow models (abstract #1588). 36th Lunar and Planetary Science Conference. CD-ROM.

Bridges F. G., Hatzes A., and Lin D. N. C. 1984. Structure, stability and evolution of Saturn's rings. *Nature* 309:333–335.

Byerlee J. D. 1978. Friction of rocks. *Pure and Applied Geophysics* 116:615–629.

Campbell C. S. 1990. Rapid granular flows. *Annual Review of Fluid Mechanics* 22:57–92.

Campbell C. S., Cleary P. W., and Hopkins M. 1995. Large-scale landslide simulations: Global deformation velocities and basal friction. *Journal of Geophysical Research* 100:8267–8283.

Carr M. H., Crumpler L. S., Cutts J. A., Greeley R., Guest J. E., and Masursky H. 1977. Martian impact craters and emplacement of ejecta by surface flow. *Journal of Geophysical Research* 82: 4055–4065.

Cook B. K. and Jensen R. P., editors. 2002. *Discrete element methods: Numerical modeling of discontinua*. Reston, Virginia: The American Society of Civil Engineers. 427 p.

Cundall P. A. and Strack O. D. L. 1979. A discrete numerical model for granular assemblies. *Géotechnique* 29:47–65.

Dartevelle S. 2004. Numerical modeling of geophysical granular flows: 1. A comprehensive approach to granular rheologies and geophysical multiphase flows. *Geochemistry Geophysics Geosystems* 5, doi:10.1029/2003GC000636.

Davies T. R. and McSaveney M. J. 1999. Runout of dry granular avalanches. *Canadian Geotechnical Journal* 36:313–320.

Dominik C. and Tielens A. G. G. M. 1997. The physics of dust coagulation and the structure of dust aggregates in space. *The Astrophysical Journal* 480:647–673.

Duran J. 2000. *Sands, powders, and grains: An introduction to the physics of granular materials*. New York: Springer-Verlag. 214 p.

Greeley R., Fink J., Snyder D. B., Gault D. E., Guest J. E., and Schultz P. H. 1980. Impact cratering in viscous targets—Laboratory experiments. Proceedings, 11th Lunar and Planetary Science Conference. pp. 2075–2097.

Hayashi J. N. and Self S. 1992. A comparison of pyroclastic flow and debris avalanche mobility. *Journal of Geophysical Research* 97: 9063–9071.

Henyey T. L. and Wasserburg G. J. 1971. Heat flow near major strike-slip faults in California. *Journal of Geophysical Research* 76: 7924–7946.

Housen K. R., Schmidt R. M., and Holsapple K. A. 1983. Crater ejecta scaling laws—Fundamental forms based on dimensional analysis. *Journal of Geophysical Research* 88:2485–2499.

Ivanov B. A. 1996. Spread of ejecta from impact craters and the possibility of estimating the volatile content of the Martian crust. *Solar System Research* 30:36–50.

Iverson R. M. 1997. The physics of debris flows. *Reviews of Geophysics* 35:245–296.

Johnson K. L. 1987. *Contact mechanics*. Cambridge: Cambridge University Press. 452 p.

Leinhardt Z. M. and Richardson D. C. 2005. Planetesimals to protoplanets. I. Effect of fragmentation on terrestrial planet formation. *The Astrophysical Journal* 625:427–440.

McGovern P. J. and Morgan J. K. 2005. Spreading of the Olympus Mons volcanic edifice, Mars (abstract #2258). 36th Lunar and Planetary Science Conference. CD-ROM.

Midi G. 2004. On dense granular flows. *The European Physical Journal E* 14:341–365.

Mouginis-Mark P. J. 1979. Martian fluidized crater morphology—Variations with crater size, latitude, altitude, and target material. *Journal of Geophysical Research* 84:8011–8022.

Mouginis-Mark P. J. 1981. Ejecta emplacement and modes of formation of Martian fluidized ejecta craters. *Icarus* 45:60–76.

Mutch P. and Woronow A. 1980. Martian rampart and pedestal craters' ejecta-emplacement: Coprates quadrangle. *Icarus* 41: 259–268.

Richardson D. C., Elankumaran P., and Sanderson R. E. 2005. Numerical experiments with rubble piles: Equilibrium shapes and spins. *Icarus* 173:349–361.

Savage S. B. and Hutter K. 1989. The motion of a finite mass of granular material down a rough incline. *Journal of Fluid Mechanics* 199:177–215.

Savage S. B. and Hutter K. 1991. The dynamics of avalanches of granular materials from initiation to runout. I. Analysis. *Acta Mechanica* 86:201–223.

Schultz P. H. 1992. Atmospheric effects on ejecta emplacement. *Journal of Geophysical Research* 97:11,623–11,662.

Schultz P. H. and Gault D. E. 1979. Atmospheric effects on Martian ejecta emplacement. *Journal of Geophysical Research* 84: 7669–7687.

Schultz P. H. and Gault D. E. 1982. Impact ejecta dynamics in an atmosphere: Experimental results and extrapolations. In *Geological implications of impacts of large asteroids and comets on the Earth*, edited by Silver L. T. and Schultz P. H. Boulder, Colorado: Geological Society of America. pp. 153–174.

Schultz P. H. and Singer J. 1980. A comparison of secondary craters on the Moon, Mercury, and Mars. Proceedings, 11th Lunar and Planetary Science Conference. pp. 2243–2259.

Stewart S. T., O'Keefe J. D., and Ahrens T. J. 2001. The relationship between rampart crater morphologies and the amount of subsurface ice (abstract #2092). 32th Lunar and Planetary Science Conference. CD-ROM.

Suzuki A., Kumagai I., Nagata Y., Kurita K., and Barnouin-Jha O. S. 2005. The formation of radial linements on fluidized ejecta (abstract #2331). 36th Lunar and Planetary Science Conference. CD-ROM.

Taylor S. R. 1982. *Planetary science: A lunar perspective*. Houston, Texas: Lunar and Planetary Institute. 481 p.

Wada K., Senshu H., and Matsui T. 2006. Numerical simulation of impact cratering on granular material. *Icarus* 180:528–545.

Wohletz K. H. and Sheridan M. F. 1983. Martian rampart crater ejecta—Experiments and analysis of melt-water interaction. *Icarus* 56:15–37.

APPENDIX: EJECTA CURTAIN MODEL

The ejecta curtain used in our calculations as an initial condition is constructed in accordance with the scaling rules of ejecta velocity distribution and cumulative ejecta volume distribution given by Housen et al. (1983), where

$$v_e(x) = k\sqrt{R_c g}\left(\frac{x}{R_c}\right)^{-\frac{1}{\gamma}} \tag{15}$$

$$V(x) = CR_c^3\left(\frac{x}{R_c}\right)^3 \tag{16}$$

and x is the radial distance from crater center, $v_e(x)$ is the ejecta velocity ejected through the surface point of x, R_c is the transient crater radius, g is the gravitational acceleration, and $V(x)$ is the ejecta volume ejected within the distance of x. The variables k, C, and γ are empirical constants, which we assume equal 0.62, 0.66, and 0.5, respectively.

First, we compute the ejecta volume excavated through the region of a crater extending from $x - \Delta x/2$ to $x + \Delta x/2$ based on Equation 16:

$$\Delta V(x) = V(x + \Delta x/2) - V(x - \Delta x/2) \tag{17}$$

where Δx is taken as the size of one ejecta particle, d_p. Then, the number of particles included in $\Delta V(x)$ is calculated by:

$$N_p(x) = \frac{\Delta V(x)}{\frac{\pi}{6}d_p^3} \tag{18}$$

Finally, we fit $N_p(x)$ particles circumferentially around the crater center by placing them one in front of the next, taking into account ejection velocities given by Equation 15.